NRL REPORT NO. R 3193

CALCULATION OF DOUBLY CURVED REFLECTORS FOR SHAPED BEAMS

FR-3193

NAVAL RESEARCH LABORATORY

WASHINGTON, D.C.

NRL REPORT NO. R 319

CALCULATION OF DOUBLY CURVED REFLECTORS FOR SHAPED BEAMS

A. S. Dunbar

Approved by:

Dr. L. C. Van Atta, Head, Antenna Research Section
Dr. J. M. Miller, Superintendent, Radio I

Problem No. 34R09-16 November 3, 1947

NAVAL RESEARCH LABORATORY
COMMODORE H. A. SCHADE, USN, DIRECTOR
WASHINGTON, D.C.

DISTRIBUTION

ONR	
Attn: Code N482	2
BuAer	
Attn: Mr. O. J. Sheel	3
Dir., USNEL	
Attn: Code 300	2
ANEES, Red Bank	1
Aeronautical Board, AREC	
Attn: Mr. L. W. Sieck	15
OinC, NRLFS, Boston	
Attn: Dr. H. Krutter	2
CO, SCEL	
Attn: Dir. of Engineering	2
OCSigO	
Attn: Ch. Eng. & Tech. Div., SIGTM-S	1
CG, AMC, Wright Field	
Attn: TSELR2C, Mr. T. J. Gibbons	2
CO, AMC, Watson Laboratory, Cambridge	
Attn: Dr. R. C. Spencer	3
CO, AMC, Watson Laboratory, Red Bank	
Attn: WLENG	1
RDB	
Attn: Library	2
Attn: Navy Secretary	2
Attn: Committee on Electronics	2
Science and Technology Project	
Attn: Mr. J. H. Heald, Ch.	2

ACKNOWLEDGEMENT

The energy relations upon which this method of calculation is based were originally formulated by L. J. Chu. The development of the formulas, through Equation (7), follows that of S. Silver's report, Double Curvature Surfaces for Beam Shaping with Point Source Feeds (reference 3). Acknowledgment is due Mr. H. F. Cogan for much of the computation for the design of the experiment reflectors.

CONTENTS

ABSTRACT

A method is described for the calculation of double curvature surfaces to produce from a point source a shaped beam of arbitrary shape in one plane and uniformly narrow in the other. It is shown that the surface so calculated is the envelope of a family of paraboloids with varying focal lengths. A sample calculation is presented, where the beam shape is that required for an airborne navigational or bombing antenna given by $G(\theta) = k \csc^2 \theta \cos\theta$. A test for the single-valuedness of a computed surface is described. Patterns are shown for experimental antennas whose reflector shapes were computed by this method. It is demonstrated that some control of the antenna pattern of such an antenna can be achieved by proper motion of the antenna feed. A discussion of errors is included in an appendix.

PROBLEM STATUS

The work described in this report was done in connection with Problem No. 34R09-16, but is of such a general character that it was felt that the method of calculation of double curvature surfaces should be published as a separate report. A termination report on Problem No. 34R09-16 will be published in the near future.

CALCULATION OF DOUBLY CURVED REFLECTORS FOR SHAPED BEAMS

INTRODUCTION

Microwave antennas for certain specialized uses are required to radiate energy in particular patterns, which in general are narrow in one plane and shaped for some special distribution of energy in the other plane. An example of such an energy distribution is the so-called $\csc^2\theta$ pattern so widely known in connection with antennas for airborne navigation and bombing systems.

An antenna to radiate such a specially shaped beam requires a reflector or lens which, together with its primary source, produces a beam having the necessary shape in the one plane and narrow in the planes transverse thereto. The required reflector surface, therefore, is one which reflects all rays falling onto it from its source parallel to a given plane. Consequently for a point source* the surface must be formed by the envelope of a system of paraboloids whose axes lie all in the same plane but at varying angles of inclination to each other and to a fixed line. The curve of intersection of the reflector with its plane of symmetry, which we shall call the "central section curve," must be adjusted to give the necessary distribution of energy for the particular shaped beam.

BEAM SHAPES FOR SPECIAL USES

The shape of the antenna pattern is determined by the special use for which the particular antenna is designed. The following cases will be considered:

Case I—Isolated Targets at Constant Altitude. Antennas designed for the detection of isolated targets, such as for a system to search out and track high-flying aircraft or for an airborne system to search out isolated ships at sea, are required to radiate energy in a $\csc^2\theta$ distribution. Consider an aircraft at altitude h above the earth, as depicted in Figure 1. The power P_r received at a point Q on the earth from the antenna in the airplane is

$$P_r \propto \frac{P_t G(\theta)}{R^2}$$

where P_t is the transmitted power, $G(\theta)$ is the antenna gain in the direction θ, and

---

* For a line source the reflector is a cylinder of such curvature as to produce the required beam shape. The method of calculation of the cylindrical reflector has been discussed by Spencer, Sichak, and others: e. g., (a) MIT Rad. Lab. Report 54-24, June 1943, Spencer, R. C. Synthesis of microwave diffraction patterns with application to $\csc^2\theta$ patterns; (b) MIT Rad. Lab. Report 624, Nov. 1944, Sichak, W. and Purcell, E. Antennas with a line source and shaped cylindrical reflector; (c) MIT Research Lab. of Electronics, Tech. Report 40, June 1947, Chu, L. J. Microwave beam-shaping antennas; (d) Silver, S. and James, H. M. Microwave antenna theory and design, McGraw-Hill, (in process).

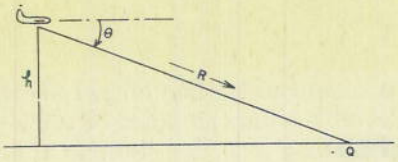

Fig. 1. Condition for Equal Energy Pattern

R is the range to point Q. Suppose an object at Q reflects some power back to the antenna, the power received by the antenna is

$$P \alpha \frac{P_t G^2(\theta) A}{R^4}$$

where A is the fraction of power reflected by the object. Now the range R is given by

$$R = \frac{h}{\sin\theta} = h \csc\theta$$

and therefore

$$G(\theta) \alpha \sqrt{\frac{h^4 P}{A P_t}} \csc^2\theta .$$

If it is further required that P be constant, then

$$G(\theta) = K \csc^2\theta \qquad (1)$$

Case II—Airborne Navigation or Bombing Systems. For an extended target such as the ground must be, the power distribution of Equation (1) does not yield uniform return to the airborne antenna. Experiment shows that $G(\theta)$ should fall off more rapidly than $\csc^2\theta$ for increasing θ. It has been shown† that for a model ground composed of a deep layer of conducting spheres of random spacing between spheres,

$$G(\theta) = K \csc^2\theta \sqrt{\cos\theta}$$

and particularly for equal brightness on a PPI scope

$$G(\theta) = K \csc^2\theta \sqrt{\operatorname{ctn}\theta} .$$

An empirical relation, however, which appears most nearly to fit the physical conditions observed in flight is

$$G(\theta) = K \csc^2\theta \cos\theta . \qquad (2)$$

Case III—Arbitrary Beam Shapes. For very specialized uses other beam shapes may be required. An antenna for a missile guidance system, for example, may require a pattern of the shape shown in Figure 2. An expression approximating such a pattern is as follows:

$$G(\theta) = e^{-k\theta^2} \Big]_{\theta_0 - \alpha}^{\theta_0 + \alpha} + k \csc^2\theta \Big]_{\theta_0 + \alpha}^{\theta \max}$$

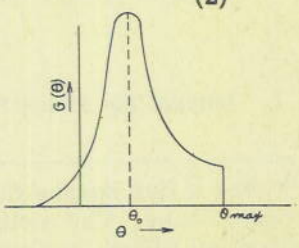

Fig. 2. Antenna Pattern of Special Shape

† MIT Rad. Lab. Report 1024, April 1946, Clapp, R. E., A theoretical and experimental study of radar ground return.

THE REFLECTOR SURFACE

The condition for the sections of the reflector surface transverse to the central section curve may be most easily formulated by considering the reflector from the point of view of reception‡. Let a sheet of rays, all parallel to the central plane (i. e., the plane of the central section curve) and lying in the plane OANP, impinge on the reflector, shown in Figure 3. We require that all rays in this plane OANP, which is perpendicular to the central plane, be brought to focus at F. Let ρ be the radius vector from F to the central section curve, ϕ its angle of depression, and β the angle between the incident and reflected rays in the central plane. Then for the optical path we have

$$AN + NF = OP + \rho$$

or, if ζ is the ordinate of N in the plane OANP with P as origin,

$$(\rho\cos\beta - \zeta) + [\,\rho^2\sin^2\beta + x^2 + (\rho\cos\beta - \zeta)^2\,]^{1/2} = \rho(1 + \cos\beta).$$

After some reduction we obtain

$$x^2 = 2\rho\zeta\,(1 + \cos\beta) \tag{3}$$

which, upon substituting a trigonometric identity, becomes

$$x^2 = 4\zeta\,(\rho\cos^2\beta/2). \tag{3a}$$

The section of the surface in the plane OANP is, therefore, a parabola. Thus given the central section curve $\rho(\phi)$, and the associated function $\beta(\phi)$, the entire reflector surface is determined.

The calculation of the central section curve is based upon geometrical optics. Referring to Figure 4, we have for the central section the differential equation

$$\frac{d\rho}{\rho d\phi} = \tan\beta/2. \tag{4}$$

Measuring ϕ positive downwards from the horizontal, we have

$$\beta = \phi + \theta. \tag{5}$$

Integrating Equation (4) we obtain an expression for $\rho(\phi)$, namely

$$\log_e \rho/\rho_0 = \int_{\phi_1}^{\phi} \tan\frac{1}{2}(\phi + \theta)\, d\phi \tag{6}$$

where ρ_0 is an arbitrary constant chosen for a convenient reflector size. Equation (6) requires that we know the correspondence between ϕ and θ in order to evaluate the integral. This is obtained by consideration of the energy relations in the primary and secondary patterns. Thus, the energy is a small cone of rays from F, defined

---

‡ MIT Rad. Lab. Report 691, June 1945, Silver, S., Double curvature surfaces for beam shaping with point-source feeds.

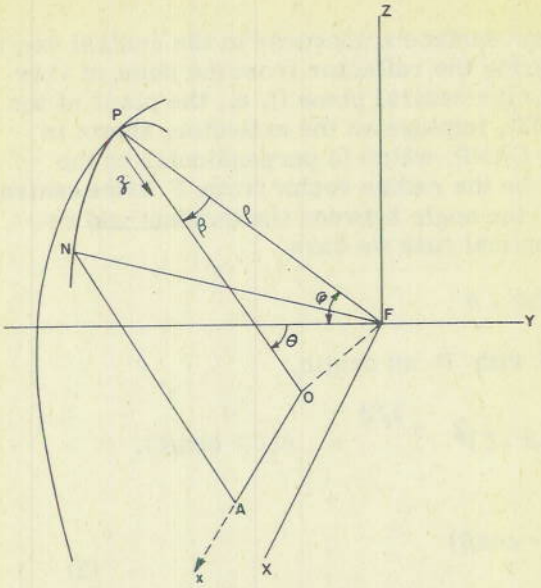

Fig. 3. Conditions for the Transverse Section of the Reflector

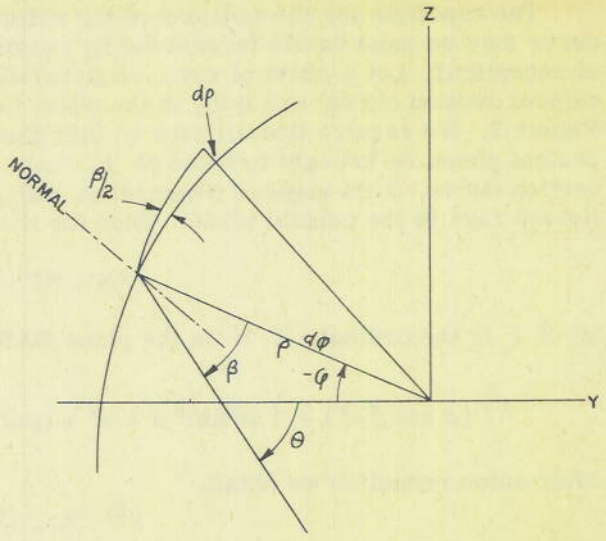

Fig. 4. Condition for the Central Section Curve

by ϕ and $\phi + d\phi$ in elevation and of width $d\psi$ in azimuth (Figure 5a), is given by

$$I(\phi)d\phi d\psi$$

where $I(\phi)$ is the power radiated per unit solid angle in the direction (ϕ, O). On reflection, this energy appears in a wedge (Figure 5b), defined by θ and $\theta + d\theta$, assuming the rays to be essentially parallel in the transverse planes. The energy in this wedge is

$$G(\theta)\rho\, d\psi d\theta.$$

Equating this to the incident energy we have

$$G(\theta)d\theta = \frac{I(\phi)}{\rho}d\phi \qquad (7)$$

which, upon integration§, will yield θ as a function of ϕ as required for solution of Equation (6). The expressions on either side of Equation (7) are normalized to their relative maxima for convenience in computation.

---

§ Taking logarithmic derivatives with respect to ϕ of (7) and substituting from (4) we get

$$\frac{d^2\theta}{d\phi^2} + \left[\tan\frac{1}{2}(\phi+\theta) - \frac{dI(\phi)}{d\phi}\Big/I(\phi)\right]\frac{d\theta}{d\phi} + \left[\frac{dG(\theta)}{d\theta}\Big/G(\theta)\right]\left(\frac{d\theta}{d\phi}\right)^2 = 0$$

which may be solved for $\theta = f(\phi)$ by a method of successive approximations; re. MIT Rad. Lab. Report 1069, April 1946, Certaine, J., Beam shaping.

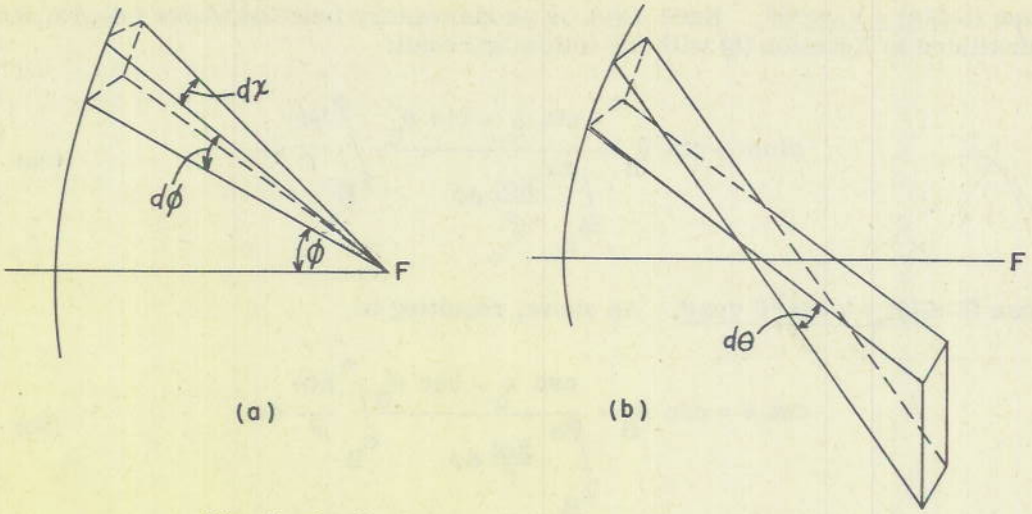

Fig. 5. On the Energy Relations in Primary and Secondary Patterns

Thus

$$\frac{\int_{\theta_o}^{\theta_B} G(\theta)\,d\theta}{\int_{\theta_o}^{\theta_B} G(\theta)\,d\theta} = \frac{\int_{\phi_B}^{\phi} \frac{I(\phi)}{\rho}\,d\phi}{\int_{\phi_B}^{\phi_A} \frac{I(\phi)}{\rho}\,d\phi} \qquad (8)$$

The limits of integration are determined by (1) the angular extent θ_o to θ_B of the idealized beam shape, and (2) the angle ϕ_A to ϕ_B subtended at the feed by the reflector's central section curve (See Figure 6).

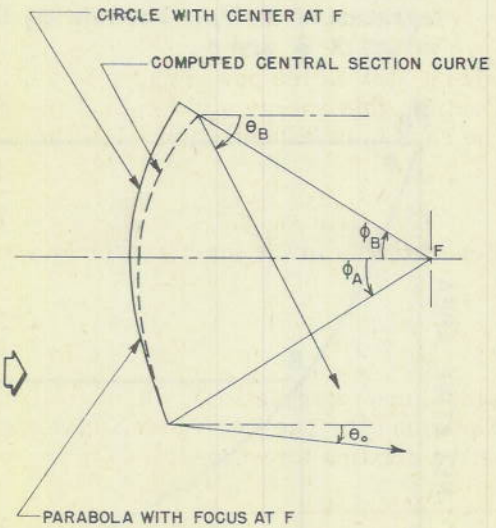

Fig. 6. Relation Between First Guess Curve and Computed Central Section Curve, Indicating Limiting Angles in ϕ and θ

INTEGRATION FOR THE VARIOUS BEAM SHAPES

The integration of Equation (8) must, in general, be performed by graphical methods. If the indefinite integral of the expression for the secondary pattern, $G(\theta)$, exists, then values of θ corresponding to values of ϕ may be computed directly from the graphical integration of $I(\phi)/\rho$. If, however, the indefinite integral of $G(\theta)$ does not exist, then both quantities must be integrated by graphical methods. The integrations for the three cases previously discussed are as follows:

Case I—$G(\theta) = k \csc^2\theta$. Here $G(\theta)$ is an elementary function whose integral may be substituted in Equation (8) with the following result:

$$\operatorname{ctn}\theta = \operatorname{ctn}\theta_B + \frac{\operatorname{ctn}\theta_o - \operatorname{ctn}\theta_B}{\int_{\phi_B}^{\phi_A} \frac{I(\phi)}{\rho}\,d\phi} \int_{\phi_B}^{\phi} \frac{I(\phi)}{\rho}\,d\phi \tag{8a}$$

Case II—$G(\theta) = k \csc^2\theta \cos\theta$. As above, resulting in

$$\csc\theta = \csc\theta_B + \frac{\csc\theta_o - \csc\theta_B}{\int_{\phi_B}^{\phi_A} \frac{I(\phi)}{\rho}\,d\phi} \int_{\phi_B}^{\phi} \frac{I(\phi)}{\rho}\,d\phi \tag{8b}$$

Case III—Arbitrary function. In order to obtain $\theta = F(\phi)$ for any function whose indefinite integral does not exist, the quantities on either side of Equation (8) are integrated graphically and plotted as shown in Figure 7. Then values of θ corresponding to values of ϕ may be read directly from the graph. Where it is desirable to expand any portion of the graph for more accurate reading, smaller increments in θ and/or ϕ may be taken for plotting on the expanded scale. The curve ABC in Figure 6 is obtained from the integration of $G(\theta)$; while the curve DEF is obtained from the integration of $I(\phi)/\rho$. The line ϕ_1 EBθ_1 represents the method of reading corresponding values of ϕ and θ.

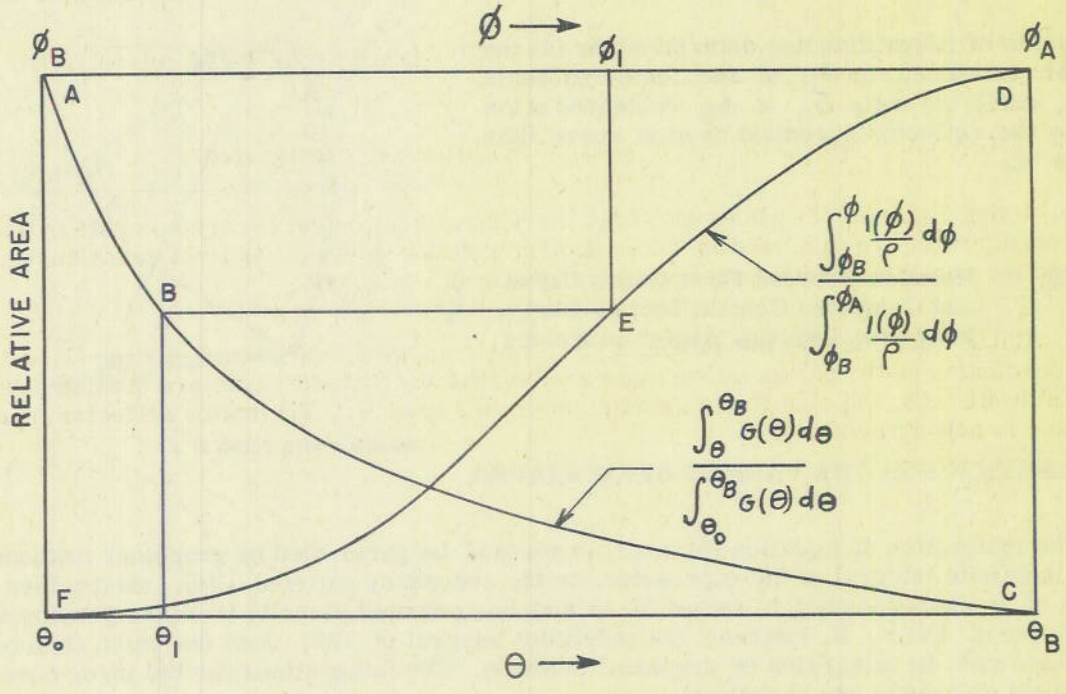

Fig. 7. Graph for Determination of $\theta = F(\phi)$

Note on graphical integrations: The integrations performed in these computations may be accomplished either by use of a planimeter or by one of the usual rules for graphical integration. It was found in most cases that the trapezoid rule provided as much accuracy and greater speed than the planimeter.

SAMPLE COMPUTATION

In the integration of $I(\phi)/\rho$ it is required that we know the function $\rho(\phi)$. It is therefore necessary that a guess be made as to the shape of the central section curve. Thus, having measured the primary pattern $I(\phi)$, we perform the integration of Equation (8) for the desired beam shape and obtain the correspondence between ϕ and θ. Then Equation (6) may be integrated graphically to obtain a solution for the central section curve. The process may be repeated by substituting the computed values of $\rho(\phi)$ into the quantity $I(\phi)/\rho$ and performing the integrations as before. In practice, no more than two such calculations are required for satisfactory accuracy in the central section curve.

In order to illustrate this method of calculation, we present the following sample calculation. Suppose that a beam shape of the form $G(\theta) = k \csc^2\theta \cos\theta$ is required for the range in θ of 5° to 55°. The vertical dimension of the reflector is chosen to be 15 inches, the focal length 14.5 inches, the horizontal width of the reflector 36 inches. A horn feed of the proper dimensions is chosen, its primary pattern in the plane of the vertical section of the reflector is carefully measured, and a guess is made as to the shape of the central section curve. This first guess curve is the so-called "barrel dish" curve, i. e., parabolic below axis, circular above, as shown in Figure 7. The computations are then performed as follows:

1. The quantity of $I(\phi)/\rho$ is plotted and graphically integrated.

2. Using Equation (8b) values of θ are computed for corresponding values of ϕ. These computations are tabulated in Table I.

3. The quantity $\tan \frac{1}{2}(\phi + \theta)$ is plotted and graphically integrated.

4. Using Equation (6) values of $\rho(\phi)$, the central section curve, are computed. These computations are tabulated in Table II. The relation between the first guess curve and the computed central section curve is shown in Figure 7.

5. Using Equation (3a) the values of $f(\phi)$ are computed, and using Equation (3) the coordinates of the parabolic sections are computed. These figures are tabulated in Table III. (Cf. the coordinate system shown in Figure 3.) The entire reflector surface is now determined.

TABLE I

Computation of θ from $\csc\theta = \csc\theta_B + \dfrac{\csc\theta_o - \csc\theta_B}{\int_{\phi_B}^{\phi_A} \frac{I(\phi)}{\rho}\,d\phi} \int_{\phi_B}^{\phi} \frac{I(\phi)}{\rho}\,d\phi$

Primary Angle ϕ	Relative Primary Power Function $\frac{I(\phi)}{\rho}$	$\int_{\phi_B}^{\phi} \frac{I(\phi)}{\rho}\,d\phi$ Square Inches	$\frac{\csc\theta_o - \csc\theta_B}{\int_{\phi_B}^{\phi_A} \frac{I(\phi)}{\rho}\,d\phi} \int_{\phi_B}^{\phi} \frac{I(\phi)}{\rho}\,d\phi$	$\csc\theta$	Secondary Angle θ
-30°	5.7	0	0	1.22078	55° 0'
27.5	7.0	.1594	.05996	1.28074	51°20'
25	9.2	.3656	.13752	1.35830	47°25'
22.5	13.1	.6531	.24566	1.46644	43°
20	19.0	1.0594	.39849	1.61927	38° 8'
17.5	27.1	1.6344	.61478	1.83556	33° 1'
15	37.6	2.4406	.91803	2.13881	27°53'
12.5	51.2	3.4281	1.28947	2.51025	23°29'
10	67.4	4.7906	1.80198	3.02276	19°19'
7.5	82.5	6.6656	2.50725	3.72803	15°34'
5	92.5	8.8531	3.33008	4.55086	12°42'
2.5	98.3	11.2375	4.22696	5.44774	10°35'
0	100.	13.7156	5.15910	6.37988	9° 1'
2.5	97.6	16.1906	6.09006	7.31084	7°52'
5	91.2	18.5593	6.98104	8.20182	7° 0'
7.5	80.8	20.7093	7.78976	9.01054	6°22'
10	65.5	22.5343	8.47623	9.69710	5°55'
12.5	49.2	23.9656	9.01461	10.23539	5°36'
15	35.8	25.0218	9.41190	10.63268	5°24'
17.5	25.5	25.7843	9.69871	10.91949	5°15'
20	17.6	26.3218	9.90089	11.12167	5°10'
22.5	12.0	26.6906	10.03961	11.26039	5° 6'
25	8.3	26.9437	10.13482	11.35560	5° 3'
27.5	6.2	27.1218	10.20182	11.42260	5° 1'
30°	4.9	27.2562	10.25237	11.47315	5° 0'

TABLE II

COMPUTATION OF CENTRAL SECTION CURVE

ϕ	θ Corrected for Continuous First Derivative	$\frac{1}{2}(\phi+\theta)$	$\tan\frac{1}{2}(\phi+\theta)$	$\int_{\phi_B}^{\phi}\tan\frac{1}{2}(\phi+\theta)\,d\phi$ Square Inches	$\log_{10}\frac{\rho}{\rho_o}$ *	ρ Inches
-30°	55° 1'	12° 30'	.22169	0	0	13.195
27.5	51° 26'	11° 57'	.21164	1.3500	.00409	13.321
25	47° 28'	11° 14'	.19861	2.6281	.00797	13.441
22.5	43° 3'	10° 16'	.18113	3.8156	.01157	13.554
20	38° 11'	9° 5'	.15988	4.8844	.01481	13.656
17.5	33° 4'	7° 47'	.13668	5.8094	.01761	13.745
15	28° 3'	6° 31'	.11423	6.5906	.01998	13.819
12.5	23° 25'	5° 27'	.09541	7.2437	.02196	13.881
10	19° 14'	4° 37'	.08075	7.7906	.02362	13.934
7.5	15° 34'	4° 2'	.07051	8.2593	.02504	13.979
5	12° 42'	3° 51'	.06730	8.6906	.02635	14.020
2.5	10° 35'	4° 2'	.07051	9.1218	.02766	14.062
0	9° 1'	4° 30'	.07870	9.5843	.02906	14.109
2.5	7° 52'	5° 11'	.09071	10.1093	.03065	14.162
5	7° 0'	6° 0'	.10510	10.7156	.03249	14.223
7.5	6° 22'	6° 56'	.12160	11.4156	.03461	14.293
10	5° 55'	7° 57'	.13965	12.2218	.03706	14.374
12.5	5° 36'	9° 3'	.15928	13.1531	.03988	14.467
15	5° 24'	10° 12'	.17993	14.2156	.04310	14.573
17.5	5° 15'	11° 22'	.20103	15.4031	.04670	14.695
20	5° 10'	12° 35'	.22322	16.7156	.05068	14.832
22.5	5° 6'	13° 48'	.24562	18.1687	.05509	14.985
25	5° 3'	15° 1'	.26826	19.7718	.05995	15.155
27.5	5° 1'	16° 15'	.29147	21.5218	.06525	15.344
30	5° 0'	17° 30'	.31530	23.4186	.07100	15.547

* $\log_{10}\frac{\rho}{\rho_o} = \int_{\phi_B}^{\phi}\tan\frac{1}{2}(\phi+\theta)d\phi$ x area factor x .43429

TABLE III

COORDINATES FOR REFLECTOR SURFACE

ϕ	β	f(ϕ)	$X \rightarrow$	0	3"	6"	9"	12"	15"	18"
-30°	25° 1'	12.576	$\zeta \rightarrow$	0	.179	.716	1.610	2.863	4.473	6.441
-27.5	23° 54'	12.749		0	.176	.706	1.588	2.824	4.412	6.353
-25	22° 28'	12.931		0	.174	.696	1.566	2.784	4.350	6.264
-22.5	20° 33'	13.124		0	.171	.686	1.543	2.743	4.286	6.172
-20	18° 11'	13.316		0	.169	.676	1.521	2.704	4.224	6.083
-17.5	15° 34'	13.493		0	.167	.667	1.501	2.668	4.169	6.003
-15	13° 3'	13.641		0	.165	.660	1.484	2.639	4.124	5.938
-12.5	10° 55'	13.756		0	.164	.654	1.472	2.617	4.089	5.888
-10	9° 14'	13.844		0	.163	.650	1.463	2.600	4.063	5.851
-7.5	8° 4'	13.910		0	.162	.647	1.456	2.588	4.044	5.823
-5	7° 42'	13.957		0	.161	.645	1.451	2.579	4.030	5.804
-2.5	8° 5'	13.992		0	.161	.643	1.447	2.573	4.020	5.789
0	9° 1'	14.022		0	.160	.642	1.444	2.567	4.012	5.777
+2.5	10° 22'	14.046		0	.160	.641	1.442	2.563	4.004	5.767
5	12° 0'	14.068		0	.160	.640	1.439	2.559	3.998	5.758
7.5	13° 52'	14.085		0	.160	.639	1.438	2.556	3.994	5.751
10	15° 55'	14.099		0	.160	.638	1.436	2.553	3.990	5.745
12.5	18° 6'	14.109		0	.159	.638	1.435	2.552	3.987	5.741
15	20° 24'	14.116		0	.159	.638	1.435	2.550	3.985	5.738
17.5	22° 45'	14.124		0	.159	.637	1.434	2.549	3.983	5.735
20	25° 10'	14.128		0	.159	.637	1.433	2.548	3.981	5.733
22.5	27° 36'	14.132		0	.159	.637	1.433	2.547	3.980	5.732
25	30° 3'	14.137		0	.159	.637	1.432	2.546	3.979	5.730
27.5	32° 31'	14.142		0	.159	.636	1.432	2.546	3.978	5.729
30	35° 0'	14.142		0	.159	.636	1.432	2.546	3.978	5.728

TEST FOR SINGLE VALUEDNESS OF THE SURFACE

It may happen that, after the central section curve has been determined and an attempt is made to develop the surface by plotting the parabolic cross sections, the surface is found to be multiple-valued in a certain region. Such a condition makes the reflector physically impossible of construction, and if it occurs a new design must be commenced. The region of multiple value is caused by the various parabolic cross sections, which are inclined at large angles to the axis, intersecting one another with the result that the surface becomes folded upon itself. The intersection of the parabolas is illustrated in Figure 8. The curve SQS' is the central section curve, CPD is a typical parabolic cross section. The parabolas passing through Q, R, and S' are seen to intersect in the regions E and F. The surface defined by these curves is multiple-valued in the region to the right of E and F. The immediate remedy for this is to reduce the horizontal aperture of the reflector until such intersection is no longer possible, but such reduction in aperture is not suitable from the point of view of preservation of azimuthal beam-width; consequently the reflector must be redesigned. Unfortunately there is no sure way to determine beforehand if the particular set of design specifications will lead to a multi-valued surface, especially if the total coverage angle, θ_0 to θ_B, is great. In general, space considerations impose the condition that the focal length should be as short as possible, so that elimination of any possibility of the surface becoming folded by simply using a long focal length is not particularly expedient. Having computed the central section curve, however, we may apply a test for the single valuedness of the surface in the following manner. By Equation (3a) the focal lengths of the transverse parabolas may be obtained, so that, knowing the horizontal aperture of the reflector, we may calculate the depth ζ of the respective parabolas from

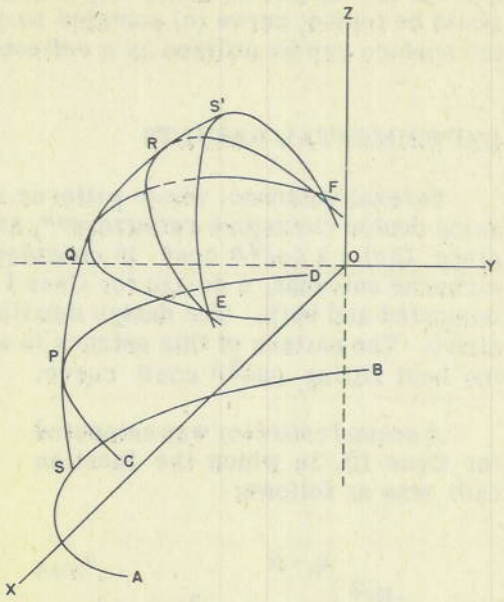

Fig. 8. Showing Intersection of Parabolic Cross Sections

$$\zeta = \frac{x^2}{4f(\phi)} \qquad (9)$$

Then plotting these depths ζ on their respective ray lines drawn in the directions θ, and connecting the points so determined, a curve is obtained which defines the contour of the extremity of the reflector surface. If this curve is single-valued (i. e., if the curve has no cusp or is not self-intersecting) the surface will be single-valued. If, however, the curve is multi-valued, the surface cannot be single-valued. Typical examples of these curves are drawn in Figure 9.

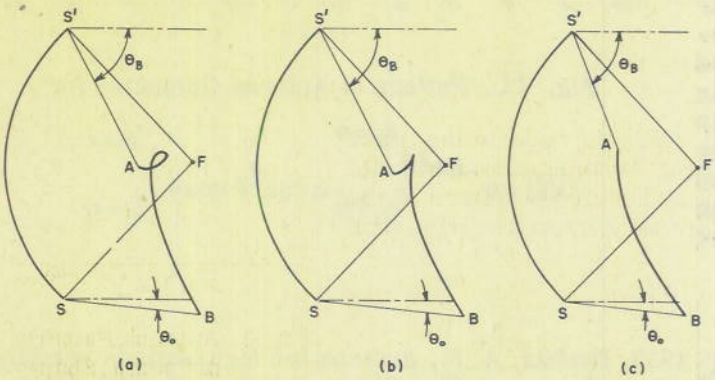

Fig. 9. Typical Examples of Curves for Test for Single-Valuedness of Surface

The curves (a) and (b) are a loop and a cusp respectively, indicating that the surfaces would be folded; curve (c) contains no singular point and is not multi-valued, showing that the surface can be utilized as a reflector.

EXPERIMENTAL RESULTS

Several antennas, whose patterns approximate $G(\theta) = k \csc^2\theta$, have been developed using double curvature reflectors**, although none were computed by this method. However, since $G(\theta) = k \csc^2\theta \cos\theta$ is considered more representative of the requirements of airborne antennas, a design for Case I was not attempted. A reflector for Case II was computed and built. The design details are those described in the sample calculation above. The pattern of this antenna is shown in Figure 10. The dotted line represents the best fitting $\csc^2\theta \cos\theta$ curve.

A second reflector was computed for Case III, in which the function $G(\theta)$ was as follows:

$$G(\theta) = e^{-K\theta^2} \Big]_{\theta_0 - \alpha}^{\theta_0 + \alpha} + k \csc^2\theta \cos\theta \Big]_{\theta_0 + \alpha}^{\theta_{max}}$$

where $\theta_0 = 3°$, $\alpha = 3°$, $\theta_{max} = 66°$. The pattern of the experimental antenna for this case is shown in Figure 11, in which the dotted line is the curve defined by the above function $G(\theta)$.

It is notable that a considerable latitude in the control of the shape of the pattern is permissible by motion of the feed away from the focus or by rotation of the feed about the focus. It is therefore possible to obtain an airborne navigational antenna, for example, whose pattern may be controlled for various altitudes and maximum ranges. Such variation in the pattern shape is illustrated in Figure 12. The reflector is the same one whose pattern for normal feed position is shown in Figure 10. The required feed motion can be realized by simple mechanical linkages.

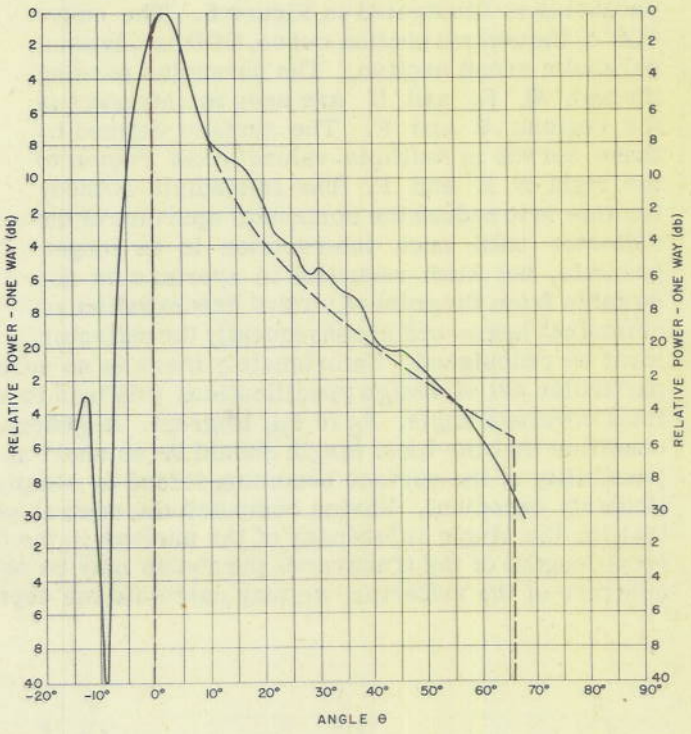

Fig. 11. Pattern of Antenna Computed for

$$G(\theta) = e^{-K\theta^2} \Big]_{\theta_0 - \alpha}^{\theta_0 + \alpha} + k \csc^2\theta \cos\theta \Big]_{\theta_0 + \alpha}^{\theta_{max}}$$

** MIT Rad. Lab. Report 411, Aug. 1943, Dunbar, A. S., Antenna for high altitude bombing (H2X); Great Britain, Telecommunications Research Establishment Report T 1878, May 1945, Hill, J. F., Macfarlane, G. G., and Walkinshaw, W. Theoretical design of a reflector to produce, from a given primary source, an arbitrary polar diagram in one plane with experimental comparison; Certaine, op. cit.

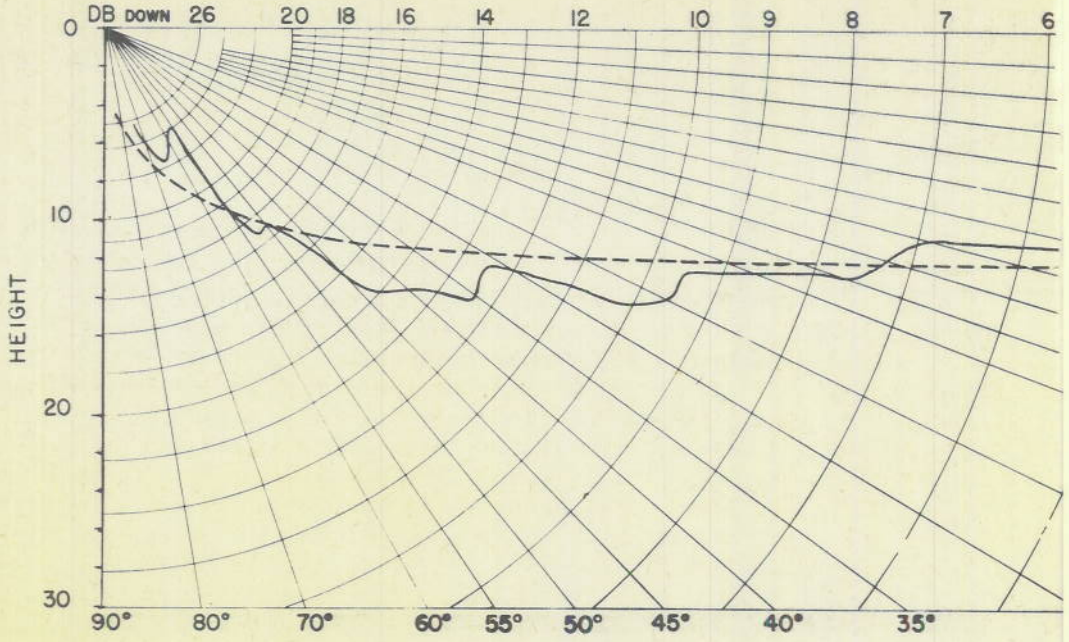

Fig. 10 - Pattern of Experimental Antenna Designed for G (θ) = K c

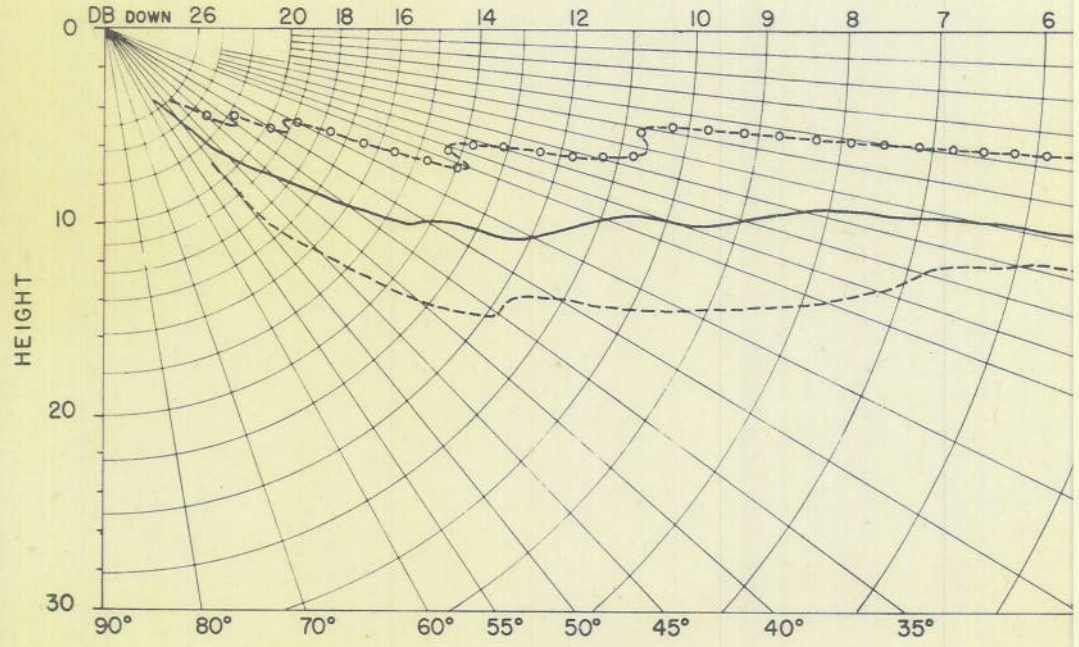

WAVE LENGTH 3.2 cm.

REFLECTOR: EXPERIMENTAL ANTENNA FOR $G(\theta) = k \csc^2\theta \cos\theta$

Fig. 12 - Control of Antenna Pattern by Feed Motion

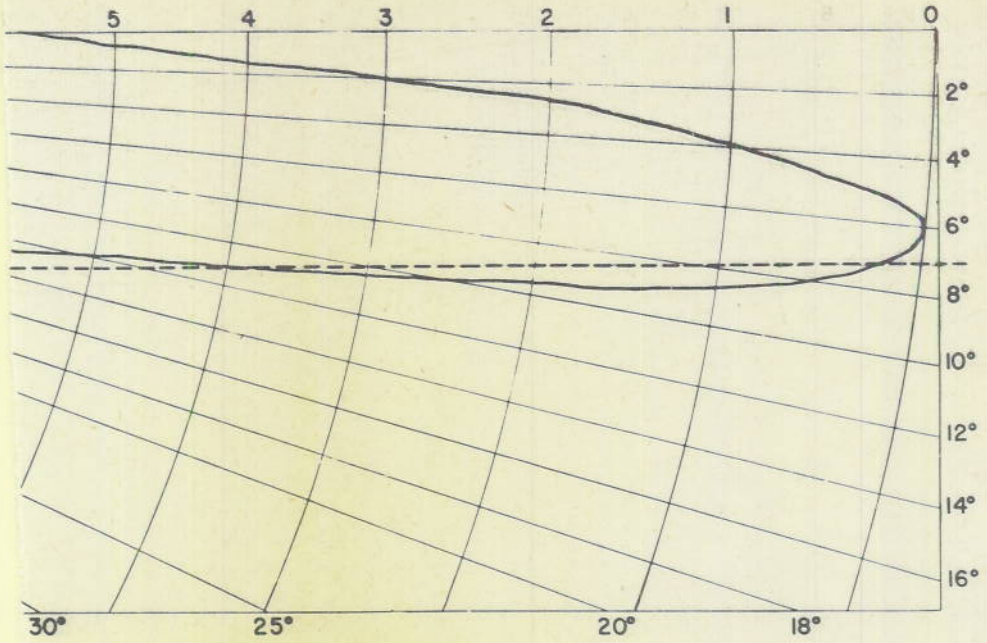

$sc^2\theta \cos\theta$

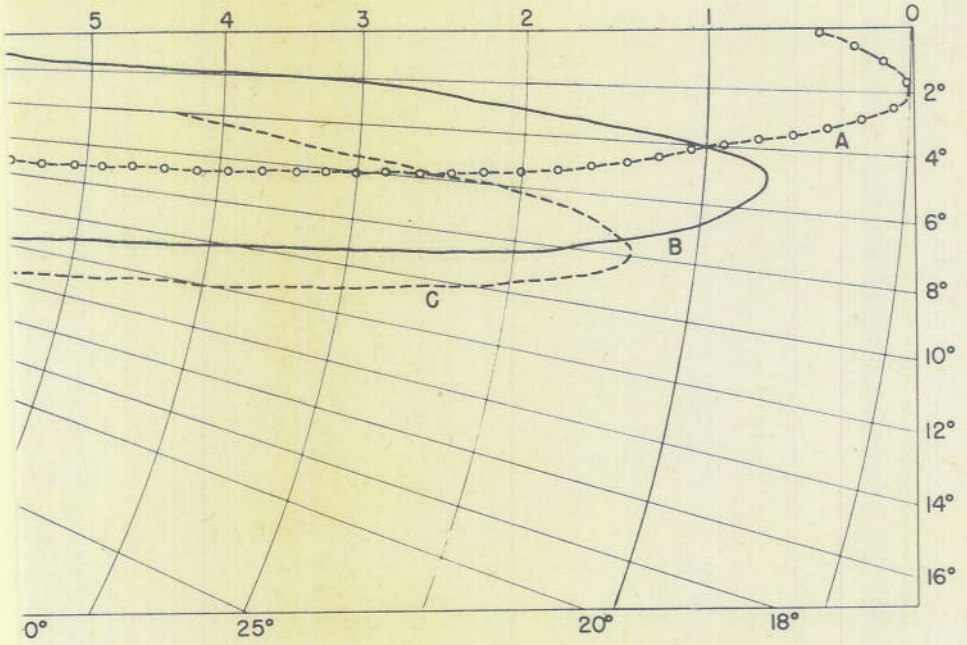

FEED: A-HORN LOWERED 3° BELOW FOCUS
B-HORN ON FOCUS
C-HORN RAISED 3° ABOVE FOCUS

ABS. GAIN: A- 31.1 db
B- 30.4 db
C- 29.7 db

APPENDIX I

DISCUSSION OF ERRORS

Suppose a certain ideal beam shape is required for a special microwave antenna application. Any antenna designed to produce this ideal beam shape will, in fact, radiate a pattern which differs from the ideal in some degree. We now define the causes of such differences as errors.

Sources of Error

The errors associated with the double curvature reflector antenna are of two general kinds: those which are mechanical, affecting the shape of the reflector surface; and those which arise from diffraction, affecting the shape of the radiated beam. The mechanical errors in the reflector surface will modify the geometrical distribution of energy and will alter, to some extent, the shape of the realized antenna pattern. The mechanical errors may be classified as (a) errors in measurement, (b) errors in computation, and (c) surface tolerances. Entirely independent of the effect of mechanical errors are the effects of diffraction. These are twofold: (a) to modify the beam shape from the ideal to an approximation to the ideal which contains no discontinuities in intensity, and (b) to superimpose diffraction lobes on the pattern.

Errors in Measurement

If the measurement of the primary feed pattern, $I(\phi)$, is in error, the reflector shape, of course, will be made incorrect for the desired secondary pattern, and consequently the antenna pattern will not have the proper distribution of power. However, since the error in measurement takes the form

$$\frac{\int_{\phi_\beta}^{\phi} \frac{I(\phi) + \Delta(\phi)}{\rho}\, d\phi}{\int_{\phi_\beta}^{\phi_A} \frac{I(\phi) + \Delta(\phi)}{\rho}\, d\phi} \qquad \text{(i)}$$

where $\Delta(\phi)$ is the relative error as a function of ϕ, it appears that errors in measurement of $\pm$ 1/2-db or less will not seriously affect the resultant antenna pattern.

Errors in Computation

Computational errors arise primarily from two sources: plotting and graphically integrating the various functions, and rounding of decimals. It may be argued that the method of calculation is not highly precise; however, precision of a sufficiently high degree may be assured by carrying all computed decimals to the fourth place. The significance of certain of these decimal places may be questioned, but assuming that in graphical integration, the area may be read to an accuracy of $\pm$1.5 percent for any small

increment, and to an accuracy of ± 0.5 percent in the total area, the maximum possible error in the computation of θ will be less than 5 minutes of arc. Similarly, the maximum error in $\log_{10} \rho/\rho_0$ is about 0.8 percent, permitting the computation of the radius vector within a maximum possible error of less than .010 inch.

Surface Tolerances

An estimate of the surface tolerances may be obtained upon consideration of Equation (4), the differential equation for the surface:

$$\frac{d\rho}{\rho} = \tan \frac{1}{2}(\phi + \theta)\, d\phi \qquad \text{(ii)}$$

Consequently, if we know the function

$$\theta = F(\phi)$$

we can evaluate the allowed increment in the radius vector ρ for a given tolerance in the direction θ; thus

$$d\theta = F'(\phi)d\phi$$

$$\Delta\rho = \rho \tan \frac{1}{2}(\phi + \theta)\ \frac{\Delta\theta}{F'(\phi)} \qquad \text{(iii)}$$

It now remains to determine $F'(\phi)$, which may be approximated by plotting the curve $\theta = F(\phi)$ and reading the slope for various values of θ. This curve for the values of θ and ϕ tabulated in Table I is shown in Figure 13.

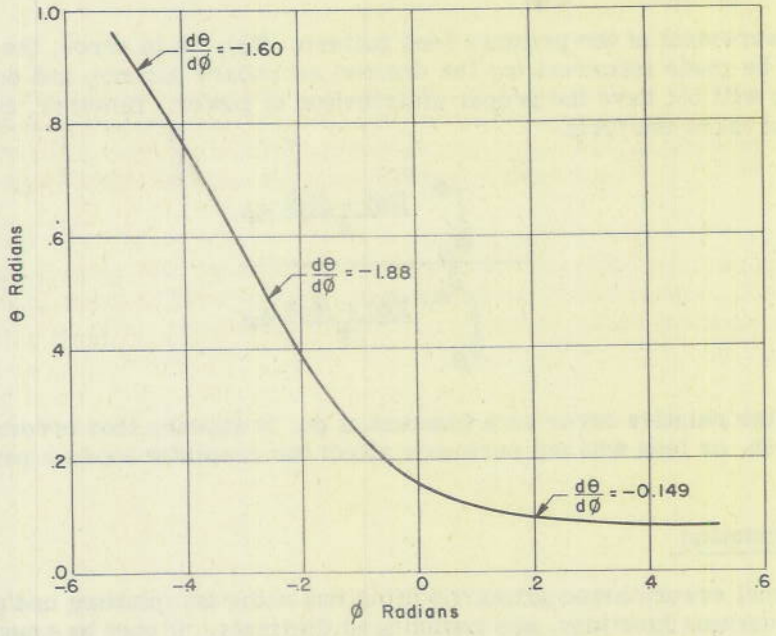

Fig. 13. Curve for $\theta = F(\phi)$

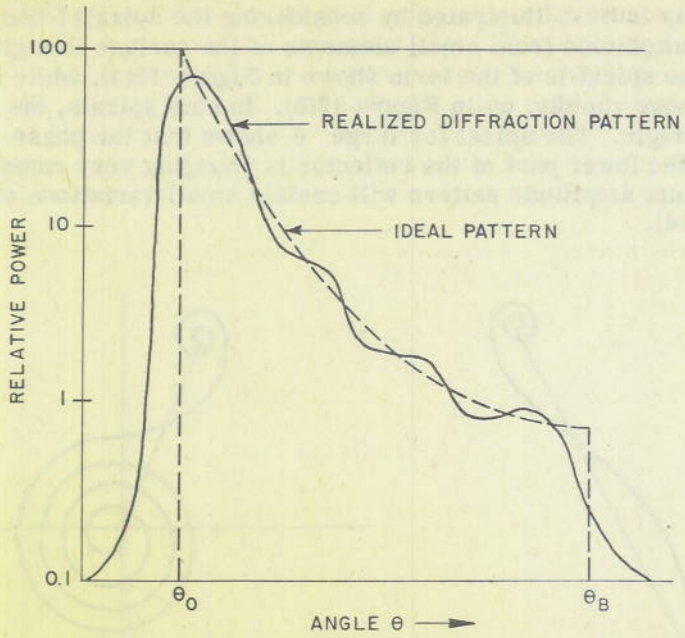

Fig. 14. Ideal and Realized Patterns

We then have to a fair degree of approximation, taking $\Delta\theta = \pm 1/4^\circ$, the following:

ϕ	θ	Slope	$\Delta\rho/\rho$	$\Delta\rho$
-27.5°	51° 20′	-1.60	.0006	.008″
-15°	27° 53′	-1.88	.0003	.004″
+12° 30′	5° 36′	-0.149	.005	.068″

Since the maximum probable error in the calculations of ρ will certainly be less than the maximum possible error, the error in ρ will be of about the same order of magnitude as (or less than) the permissable error obtained in the above calculations. It should be noted further that diffraction will most probably permit some relaxation of the surface tolerances, perhaps as much as 25 percent. The whole question of precision of the method, however, may be submerged in the comparative excellence of the experimental results.

Effect of Diffraction

The primary effect of diffraction in modification of the beam shape is the removal of sharp discontinuities in intensity. In addition small diffraction lobes are superimposed on the pattern. A comparison of the ideal and realized diffraction patterns is shown in Figure 14, for the case $G(\theta) = k \csc^2\theta$. The effect of diffraction is also illustrated in Figure 11.

The diffraction lobes in the pattern arise chiefly from the lower edge of the reflector

(Cf. Figure 7). This is best illustrated by considering the spiral†† that results from the vector additions of amplitude from small elements of the surface in a given direction θ. For θ near θ_0, the spiral is of the form shown in Figure 15(a), while for large θ, the spiral curls much more rapidly, as in Figure 15(b). In both spirals, the lower edge of the reflector is at the origin. The spiral for large θ shows that the phase of the amplitude contributions from the lower part of the reflector is changing very rapidly, and consequently the resultant amplitude pattern will contain small variations of a quasi-periodic nature (Cf. Figure 14).

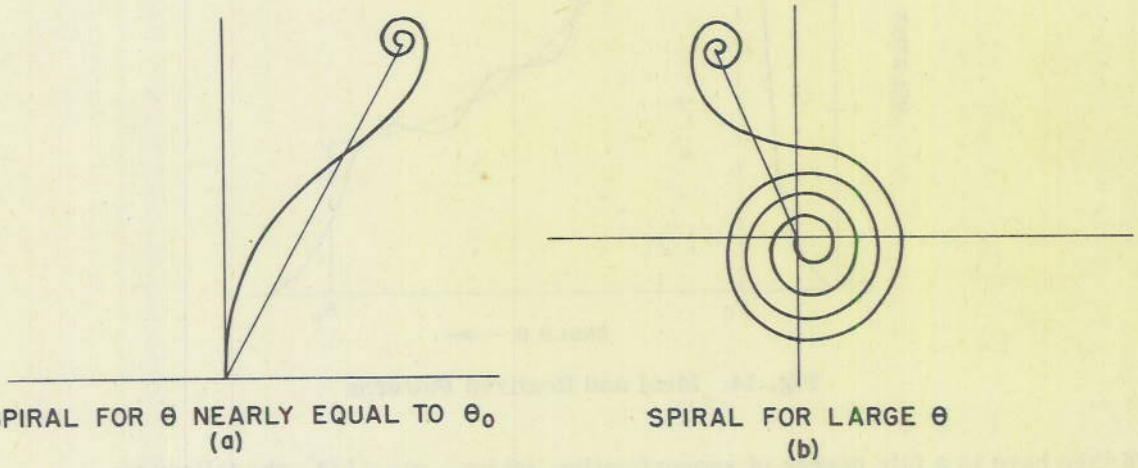

Fig. 15. Spirals Resulting From Vector Addition of Amplitude, Contributions From Elements of Reflector Surface

If an ideal pattern is assumed which is more nearly physically realizable, the agreement between the ideal pattern and the diffraction pattern is quite good. Such a case is illustrated in Figure 11, where the ideal pattern assumes a peak of the form $e^{-k\theta^2}$, which is in good agreement with the realized diffraction pattern.

---

†† MIT Rad. Lab. Report 750, Sept. 1945, Keary, T. J. Calculation of vertical polar diagrams and power gains of antennas for airborne navigational radars. This report contains computations of patterns for cylindrical reflector shaped beam antennas.